Ultrahigh Throughput and Efficient Separation of Oil/Water Mixtures Using Superhydrophilic Multi-Scale CuBTC-Coated Meshes

Wua, Chao; Zhanga, Yao; Zhao, Qi; Li, Yun; Zhang, Baoquan

Published in:
Separation and Purification Technology

DOI:
10.1016/j.seppur.2021.119802

Publication date:
2021

Wua, Chao et al. "Ultrahigh Throughput and Efficient Separation of Oil/Water Mixtures Using Superhydrophilic Multi−Scale CuBTC−Coated Meshes". Separation and Purification Technology. 2021. 279. https://doi.org/10.1016/j.seppur.2021.119802

Ultrahigh Throughput and Efficient Separation of Oil/Water Mixtures Using Superhydrophilic Multi-Scale CuBTC-Coated Meshes

Chao Wu[a], Yao Zhang[a], Qi Zhao[b,*], Yun Li[a], Baoquan Zhang[a,*]

[a] *State Key Laboratory of Chemical Engineering, School of Chemical Engineering and Technology, Tianjin University, 135 Ya Guan Road, Jinnan District, Tianjin, 300350, China*

[b] *School of Science and Engineering, University of Dundee, Nethergate, Dundee, DD1 4HN, UK*

*Corresponding Authors. Tel: +86 13802180732. E-mail addresses: bqzhang@tju.edu.cn (B. Zhang), q.zhao@dundee.ac.uk (Q. Zhao)

ABSTRACT: High-flux and oil-resistant mesh for oil/water separation is substantially needed due to frequent oil spill accidents. However, the acquirement of high-flux meshes without sacrificing intrusion pressure is a challenge. Here, a multi-scale CuBTC-coated copper mesh was prepared via a novel stepwise liquid-phase epitaxial (LPE) procedure and secondary growth. On the basis of the uniform CuBTC seed layer on the surface of copper mesh via the LPE method, the micro-scale CuBTC coating was obtained by secondary growth. The nanosized CuBTC humps were further fabricated on the surface of micro-scale CuBTC crystals to form the multi-scale structure. The as-prepared multi-scale CuBTC-coated mesh possessed superhydrophilicity and underwater superoleophobicity. The stabilities and anti-fouling behavior of the as-prepared CuBTC-coated mesh were investigated. In addition to high oil/water separation efficiency (over 99%), the multi-scale CuBTC-coated mesh exhibited unprecedentedly high permeation flux (180.6 $L \cdot m^{-2} \cdot s^{-1}$) with a satisfactory oil intrusion pressure (2.2 kPa), demonstrating its application potential for quick oil-spill cleanup.

Keywords: Multi-scale; CuBTC; Superhydrophilicity; Liquid-phase epitaxial; Oil/water separation

1. Introduction

Oil/water separation has become a global topic due to frequent oil spill accidents worldwide. There exists an urgent need to develop efficient approaches for cost-effective and convenient separation of oil/water mixtures [1,2]. Since oil/water separation is an interfacial process, the design and application of supported coatings with special wettability could play a key role in practical applications. Until now, a variety of supported coatings with special wettability have been fabricated on metallic meshes possessing hierarchal rough surface as well as appropriate surface energy [3−7].

Inspired by the remarkable oil-repellent characteristic of fish scales in aqueous media, superhydrophilic and underwater superoleophobic materials with high water affinity and extremely low oil adhesion have been fabricated on metallic meshes, including polyacrylate-grafted poly(vinylidene fluoride) [8], palygorskite [9], NiO [10], zeolite [11], silver (Ag) [12], poly(ionic liquid) (PIL) [13], crosslinked ionic polymer (CIP) [14], and graphene oxide (GO) [15], Fe^{III}-phytic acid [16], UIO-66 [17,18], polydimethylsiloxane (PDMS) [19], and ZnO [20]. However, a high flux could be achieved at a decreased intrusion pressure and vice versa. Li et al. assembled superhydrophilic phytic acid metal complexes on stainless steel mesh (SSM) and obtained a high water flux of 175 L m^{-2} s^{-1} by increasing mesh pore size, while the intrusion pressure was reduced to an extremely low level (0.2 kPa) [16]. A larger pore size results in a higher flux, but the intrusion pressure would be further reduced. Figure S1a summarizes the experimental results in recent literature reports [9–14,16–20]. Clearly, the flux of water cannot be enhanced without a sacrifice of oil intrusion pressure with a trade-off behavior between water flux and oil intrusion pressure. According to Young–Laplace equation [21]

$$P = -\frac{4\gamma_{\mathrm{ow}} \cos\theta_{\mathrm{ow}}}{d} \quad (1)$$

where P is the intrusion pressure, d the mesh pore size, γ_{ow} the interface tension of oil/water, θ_{ow} the underwater oil contact angle (UOCA). Increasing θ_{ow} can neutralize the adverse effect of an enlarged pore size on the intrusion pressure. In general, the wettability of a solid surface greatly depends on its chemical composition and geometrical structure. When oil droplets come in contact with a hydrophilic surface underwater, water pockets would be formed on the rugged micro-structure [22]. As shown in Figure S1b, these water pockets between pillars would greatly reduce the contact area between the oil and solid surface, and thus give rise to a large UOCA.

When the pore size is too large to form a strong water film, air replaces some of the trapped water in pockets, resulting in a change in the three-phase interface and the invalidity of eq 1. Therefore, the simultaneous enhancement of both water flux and oil intrusion pressure under a relatively large pore size could be achieved by generating a continuous and strong water film and increasing the UOCA as much as possible.

Metal-organic frameworks (MOFs) are a class of crystallized porous materials formed by the coordination of metal ions/clusters and organic bridging materials. It is believed that hydrophilic MOF coating with micro-scale rough structures could create water pockets when immersed into water (Figure S1c). More significantly, the extremely abundant pore structures of MOFs would be filled with water under capillarity, thus a stronger and thicker water film could be formed compared with other hydrophilic coatings. Besides, contrasted to single-scale rough structures, multi-scale structures formed by the integration of micro-scale and nano-scale architectures could further increase the surface roughness, which reduces the contact area between oil and solid surface and thus gives rise to a larger UOCA (Figure S1d). Therefore, increasing the mesh pore size and meanwhile fabricating superhydrophilic MOF coating with multi-scale micro-/nano-structures is a feasible strategy to design high-flux meshes with an appreciable oil intrusion pressure.

In this work, copper mesh supported superhydrophilic CuBTC coating with multi-scale hierarchical structures will be designed and constructed to achieve an unprecedented performance for oil/water separation as follows, where CuBTC is selected due to its high affinity to water.

2. Design and Construction of Superhydrophilic Multi-Scale CuBTC-Coated Meshes

CuBTC (also known as HKUST-1) was chosen as the coating material because of its high affinity to water [23,24]. Guo et al. prepared CuBTC-coated SSMs by using polydopamine as a binder, however, the CuBTC crystals just stacked on the SSM loosely and fell off easily [25]. A well-intergrown and rugged CuBTC coating anchored tightly on mesh wire is highly desired. It is preferable to choose copper mesh for separating substrate as it can offer copper source for the nucleation of CuBTC, thus enhances the anchoring force between the coating and mesh [26]. Besides, the secondary growth method has been proved to be an effective method for preparation of intergrown ZIF-8 coating on SSM, in which polyethyleneimine was used to bind seed crystals [27]. The key step for the secondary growth is to fix small nano-sized MOF seeds onto the mesh surface. However, due to the relatively slow nucleation rates and fast growth kinetics, CuBTC usually has large particle sizes with broad size distributions, which leads to the non-uniform seed layer [28]. Herein, we propose a novel approach to prepare uniform CuBTC seed layers on copper meshes by using a stepwise liquid-phase epitaxial (LPE) technique, in which no binding agent will be used. Based on the uniform CuBTC seed layer, a single micro-scale CuBTC coating will be prepared by secondary growth. Then, the LPE technique will be used once again to fabricate nano-sized CuBTC humps on the surface of micro-sized CuBTC crystals, leading to the formation of multi-scale micro-/nano-structures. Therefore, to construct superhydrophilic multi-scale CuBTC-coated meshes, a uniform CuBTC seed layer needs to be prepared at first, followed by the fabrication of CuBTC coating with multi-scale micro-/nano-structures.

2.1. Preparation of uniform CuBTC seed layer on copper meshesby LPE technique

In order to provide nucleation sites for CuBTC on mesh surface, the copper mesh was calcined for oxidation firstly, meanwhile, hydroxyl groups were introduced after oxidation. Next,

Cu^{2+} solution and H_3BTC solution were separated from each other and the calcined mesh was deposited with them in a stepwise and repetitive, cyclic manner. H_3BTC molecules were first grafted on the mesh surface via covalent bond between the carboxyl groups on H_3BTC and the hydroxyl groups introduced after calcination. Besides, some carboxy groups on H_3BTC chelated with Cu^{2+} on the mesh directly. A portion of the carboxyl groups on H_3BTC played a role of binder, and the residual carboxyl groups linked with Cu^{2+} during next deposition. Every Cu^{2+} ion simultaneously chelated with two carboxyl groups enabled CuBTC crystals to nucleate and grow. A uniform seed layer would be prepared after cycling seven times. This fabrication process is shown in Scheme 1, while the detailed preparation process of multi-scale CuBTC-coated meshes are given in the next section.

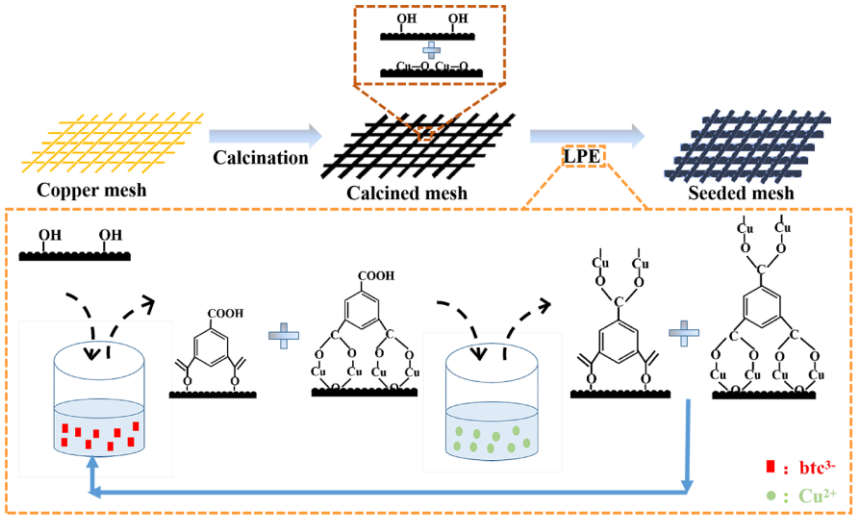

Scheme 1. Fabrication of uniform CuBTC seed layer on copper meshes via LPE seeding procedure.

2.2. Preparation of multi-scale CuBTC-coated meshes

Following the usual routine of the secondary growth method, the obtained CuBTC seeded mesh was solvothermally treated further, and the nanosized seed layer would grow into

intergrown micro-scale CuBTC coating with rough micro-structures. Theoretically, the crystal growth rate of CuBTC could be controlled precisely by the above mentioned stepwise LPE technology. Thus, the LPE technology was used again to assemble nanosized CuBTC crystals on the surface of single micro-scale CuBTC coatings, leading to the formation of multi-scale CuBTC coatings with micro-/nano-structures. A schematic illustration of the process is shown in Scheme 2.

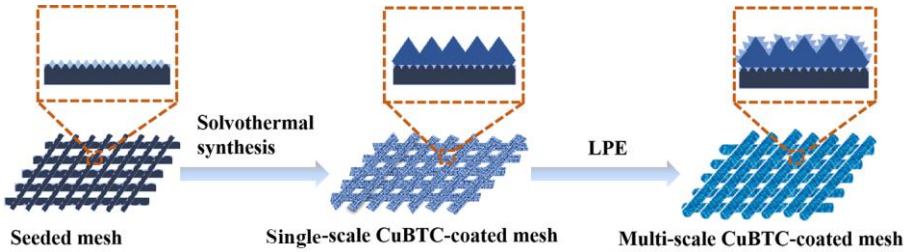

Scheme 2. Fabrication of multi-scale CuBTC-coated meshes.

3. **Experimental**

3.1. Materials

The copper mesh (mesh number 200) was purchased from local market. Trimesic acid ($C_9H_6O_6$, 98%), copper nitrate trihydrate ($Cu(NO_3)_2 \cdot 3H_2O$, 98%) and copper acetate monohydrate ($Cu(CH_3COO)_2 \cdot H_2O$, 99%) were purchased from Shanghai Macklin Biochemical Co., Ltd., China. Ethanol (99.5%), dichloromethane (99.5%), *n*-hexane (99.5%), tetrahydrofuran (99.0%), dimethylformamide (99.5%), N-methylpyrrolidone (99.0%), trichloromethane (99.0%), and methylblue were purchased from Tianjin Kermel Chemical Co., Ltd., China. Petroleum ether (99.9%) was purchased from Tianjin Fuchen Chemical Co., Ltd., China. Sudan I was purchased from Shanghai Yuanye Chemical Co., Ltd., China. All chemicals and solvents were used as received without further purification. Deionized water (DI water) was obtained from a

water purifier (Ulpure-II-10 T, Chengdu Ultrapure Technology Co., Ltd.) with a resistivity of 18.25 MΩ·cm.

3.2. Preparation of CuBTC seed layer

The cooper mesh (3 cm × 3 cm) was cleaned in acetone, ethanol and DI water in ultrasonic cleaner (40 Hz), respectively, and then calcined under 600 °C for 20 min for oxidization. The cooper mesh after calcination was seeded by a stepwise LPE technique. The mesh was immersed under ultrasonic irradiation in 8 mM ethanolic solution of H_3BTC for 40 min at first. Then the mesh was immersed in 10 mM ethanolic solution of $Cu(CH_3COO)_2 \cdot H_2O$ in next step for 40 min. Unreacted or physisorbed components were removed between successive deposition steps by rinsing with ethanol. After the deposition procedure was repeated seven times, these meshes were dried at 60 °C for 30 min to prepare them for the synthesis of the intergrown CuBTC coating.

3.3. Preparation of multi-scale CuBTC-coated mesh

The above obtained seeded mesh was vertically immersed at the bottom of an autoclave with 25 ml ethanol solution of 1.5 mmol H_3BTC and 2 mmol $Cu(NO_3)_2 \cdot 3H_2O$. After crystallized at 120 °C for 24 h, the single micro-scale CuBTC-coated mesh was taken out and washed with ethanol three times. Then, the single scale CuBTC-coated mesh was immersed in 8 mM H_3BTC solution and 10 mM $Cu(CH_3COO)_2 \cdot H_2O$ solution sequentially for 40 min. After repeating this immersion procedure three times, multi-scale CuBTC-coated mesh was obtained.

3.4. Characterization

The crystalline structures of the prepared samples were analyzed by X-ray diffraction (XRD) using a Bruker axs D8-Focus equipped with Cu Kα radiation. Measurements were performed in a range of Bragg's angles 2θ = 2–50° at a scanning rate of 8°/min. The morphologies of these

samples were obtained via scanning electron microscopy (SEM, Hitachi S-4800). The contact angle (CA) was measured with the Dataphysics OCAH 200 instrument at ambient temperature. For static CAs of water in air (WCAs), liquid droplets (5 μL) were directly put on the mesh. For UOCA measurement, the samples were firstly fixed in a container that was transparent and filled with water.

3.5. Oil/water separation

The obtained meshes were used to separate oil/water mixtures in a homemade setup. One piece of mesh was horizontally fixed between the ends of two vertical glass tubes. Before separation, the prepared mesh was firstly wetted by water. Water and oil were mixed in a volume ratio of 50 %, with oil and water dyed with Sudan I and methylblue respectively for clear observation. The prepared oil/water mixtures were poured onto the mesh and water spontaneously permeated quickly under gravity force. The separation efficiency was defined according to $\eta\,\% = (m_1/m_0) \times 100$, for which m_0 is the mass of oil before separation process and m_1 is the mass of oil intercepted in the upper tube.

Water flux test resembled to the process of oil/water separation. 300 mL DI water was poured into the upper tube of the device, and the time of the water to pass through the mesh completely was measured. When oil intrusion pressure was tested, the as-prepared mesh was prewetted by water and fixed in the above device. Then, dyed *n*-hexane was added into the upper tube dropwise until the mesh could not support, and the maximum height of the oil was measured.

4. **Results and discussion**

4.1. Multi-scale CuBTC-coated meshes

As mentioned above, the copper mesh was used as the separating substrate because it could offer copper source for the nucleation of CuBTC, thus enhanced the binding forces between the

coating and mesh. As shown from Figure 1a–c, the pristine copper mesh had an average pore size of ca. 75 μm with smooth surface. After washing, this copper mesh was calcined for oxidation, monitored by the color from yellow to black, and the smooth surface became rough and rugged (Figure S2a–c). To prepare uniform CuBTC seed layer on the calcined copper mesh, a stepwise LPE technique was adopted in which no binding agents were used. The basis of the LPE technique was that the reaction components were combined in a sequential manner. Unreacted or physisorbed components were removed between successive deposition steps by rinsing with ethanol. The stepwise synthesis endowed the rate of crystal growth with a good control, thus nanosized CuBTC seed particles were evenly grafted on the mesh surface as shown in Figure S2d–f, which would supply a good stand for the following secondary growth process. It is notable that this simple LPE technique does not require any chemical surface modification and allows large-scale preparation of these CuBTC seeded mesh, given that copper meshes are commercially available. Subsequently, the seeded mesh was solvothermally treated, and a highly compact micro-sized CuBTC coating with a ridge and valley like rough structure was obtained, and the average pore size of the mesh was reduced to ca. 65 μm (Figure 1d and e). The magnified SEM image given in Figure 1f demonstrated the surface of micro-scale CuBTC crystals was extremely smooth. To further enhanced the surface roughness, nanosized CuBTC humps were fabricated on the single micro-scale CuBTC coatings by LPE technique (Figure 1g–i). The ridge and valley like CuBTC on the micro-scale and the hump-shaped CuBTC on the nano-scale together constituted a multi-scale CuBTC coating with a hierarchical micro-/nano-structures. In addition, XRD patterns of bare calcined copper meshes and multi-scale CuBTC-coated meshes were shown in Figure S3. The peak positions in the XRD pattern of the prepared mesh matched well with those of the simulated patterns, indicating the phase purity of the

polycrystalline multi-scale CuBTC coating. As speculated, such multi-scale micro-/nano-structures can amplify the surface wetting performance, and it is expected that particular wetting performances can be observed on multi-scale CuBTC-coated mesh.

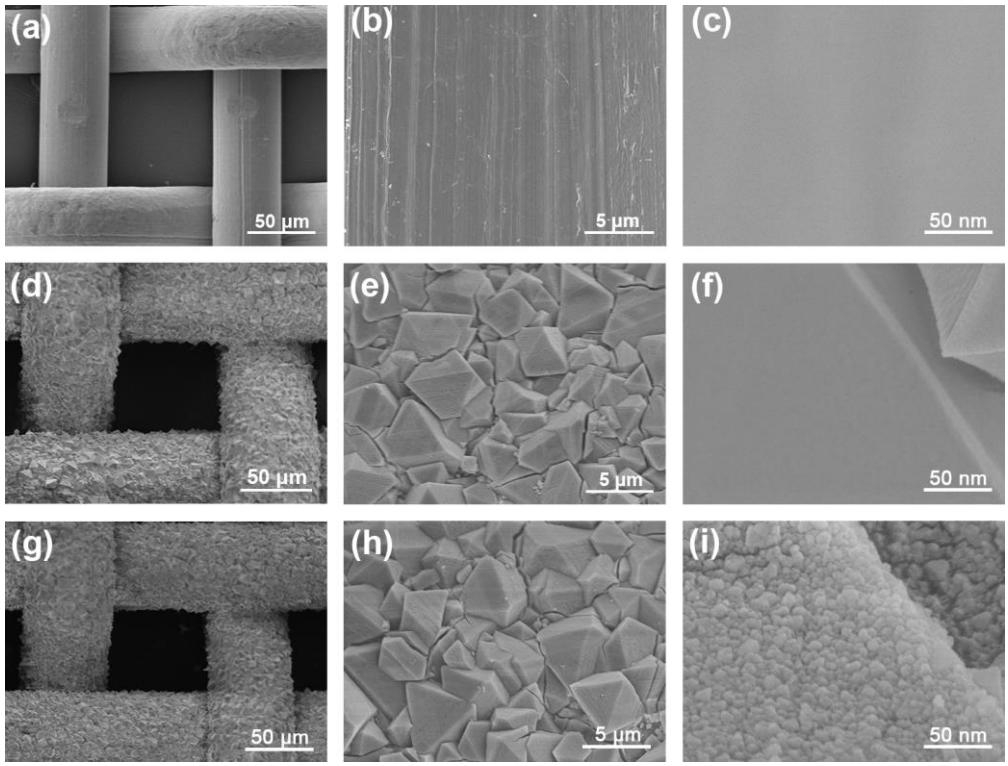

Figure 1. SEM images of pristine copper mesh (a, b and c), single-scale CuBTC-coated mesh (d, e and f), and multi-scale CuBTC-coated mesh (g, h, and i).

4.2. Surface wettability of multi-scale CuBTC-coated meshes

To evaluate the water and oil wettability of these meshes, we conducted CA measurements in air and under water. In air, the WCA of the original copper mesh was 123° (Figure 2a), however, the WCA of calcined mesh was reduced to 34° as a result of introduced hydroxyl groups and improved surface roughness (Figure S4a). Naturally, both single-scale CuBTC-coated mesh and multi-scale CuBTC-coated mesh exhibited excellent superhydrophilicity with a WCA of ca. 0° (Figure 2b and c), which was attributed to the massive hydrophilic carboxylate groups and rough

hierarchical structure of CuBTC coatings. As for oil wettability under water of these meshes, the UOCA of the original copper mesh was 54° (Figure 2d), however, the UOCA of calcined mesh was increased to 135° (Figure S4b) as a result of improved hydrophilicity and surface roughness. After micro-scale CuBTC-coated mesh immersed in water, water pockets formed on the rugged micro-structure because of inherent hydrophilicity of CuBTC. Theses water pockets greatly reduced the contact area between the oil and mesh surface, and thus resulted a large UOCA of about 154° (Figure 2e). Remarkably, after nanosized CuBTC humps were fabricated on the surface of micro-sized CuBTC crystals, which further enhanced the roughness of coatings. For this multi-scale CuBTC-coated mesh, the contact area between the oil and solid surface underwater was reduced to smaller and thus gave rise to a larger UOCA of 162°, confirming a great improvement of underwater superoleophobicity (Figure 2f). Based on the WCA and UOCA results, it is safe to conclude that a mesh with excellent superhydrophilicity and underwater superoleophobicity was achieved by designing a multi-scale CuBTC coating. The multi-scale CuBTC-coated meshes can find great applications in oil/water separation.

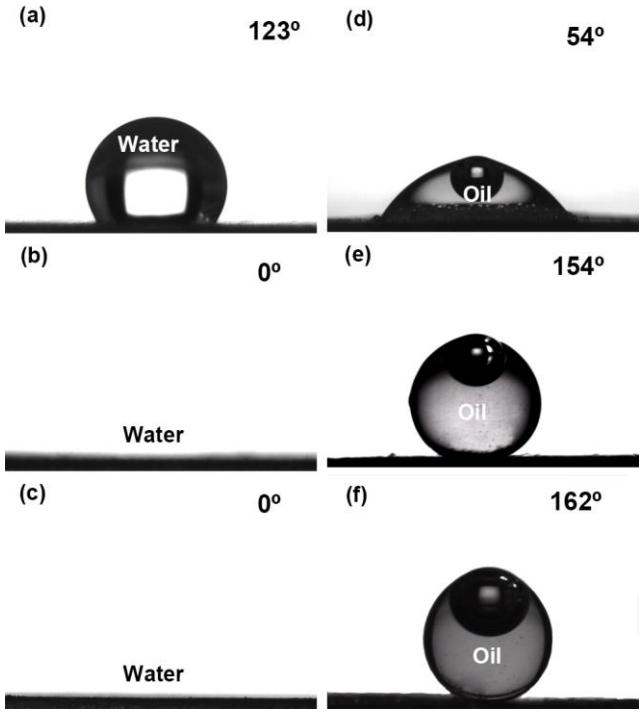

Figure 2. Special wettability behaviors. Photographs of a water droplet (a) and an underwater oil droplet (b) on pristine copper meshes, a water droplet (c) and an underwater oil droplet (d) on single-scale CuBTC-coated meshes, and a water droplet (e) and an underwater oil droplet (f) on multi-scale CuBTC-coated meshes. The used oil in these measurements is dichloromethane.

4.3. Separation and stability performances

A series of proof-of-concept experiments were carried out to evaluate the oil/water separation ability of our mesh. A mixture of *n*-hexane and water was poured onto the water prewetted mesh that was fixed between the two glass tubes (Figure S5). The only force driving the oil and water separation was the weight of the liquid itself. Owing to the outstanding superhydrophilicity and underwater superoleophobicity of multi-scale CuBTC-coated mesh, water possessing a larger gravitational force than oil passed through the mesh quickly while the *n*-hexane was maintained above the mesh. The separation efficiency of multi-scale CuBTC-coated mesh for *n*-

hexane/water mixture was measured to be above 99.5%. Analogously, the mesh could selectively separate various oil/water mixtures, such as petroleum ether, *n*-heptane, and toluene. As shown in Figure 3a, the separation efficiencies of multi-scale CuBTC-coated meshes were all above 99% for different oil/water mixtures.

In addition to the separation efficiency, water flux is significant for the performance of oil/water separation, especially for the purpose of quick clearance of spilled oil. Water flux F ($L \cdot m^{-2} \cdot s^{-1}$) was calculated by measuring the time of 300 mL water to pass through the mesh based on the following equation:

$$F = \frac{V}{St} \tag{2}$$

where V is the volume of water that permeates through the mesh, S the effective area of the mesh, and t the required time for water to pass through. Here, water flux for the prepared multi-scale CuBTC-coated mesh was 180.6 $L \cdot m^{-2} \cdot s^{-1}$, which was quite high for water-permeating oil/water separation mesh.

To further study the separation ability of the meshes, oil intrusion pressure P (kPa) was also obtained by measuring the maximum height of oil that the mesh could support. The experimental intrusion pressure value was calculated using the following equation:

$$P = \rho g h \tag{3}$$

where P is the experimental intrusion pressure, ρ the density of *n*-hexane, g the acceleration due to gravity, and h the maximum height of *n*-hexane that the mesh can endure. The calculated intrusion pressure of *n*-hexane for calcined copper mesh and multi-scale CuBTC-coated mesh were 772 Pa (denoted as P_1) and 2.2 kPa (denoted as P_2), respectively (Figure S6).

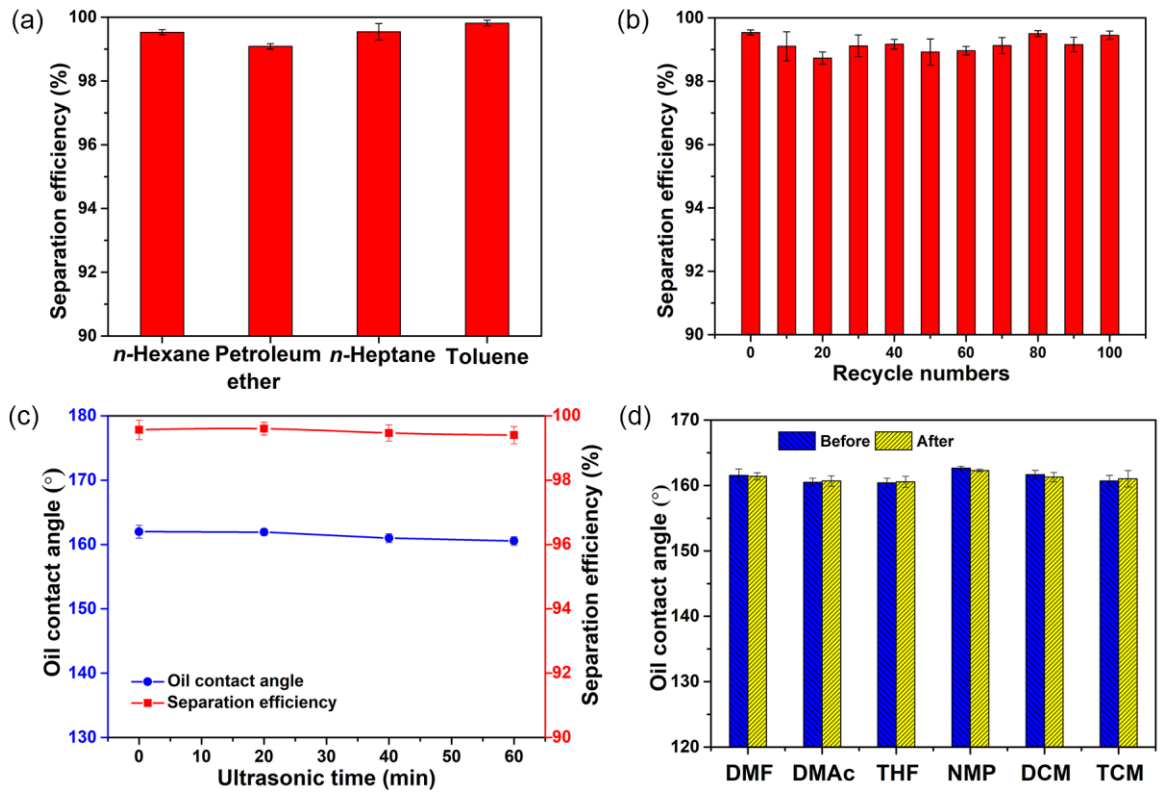

Figure 3. (a) Separation efficiency of the multi-scale CuBTC-coated mesh for various oil/water mixtures. (b) The *n*-hexane/water separation efficiency after different recycle numbers. (c) UOCAs and *n*-hexane/water separation efficiency with respect to ultrasonic time. (d) UOCAs of the prepared mesh before and after immersing in various organic solvents for 24 h.

Apart from the flux and separation efficiency, the cycling and stability of multi-scale CuBTC-coated meshes are also essential for oil/water separation. As seen from Figure 3b, multi-scale CuBTC-coated meshes still retained their underwater superoleophobicity after 100 separation cycles with separation efficiencies for *n*-hexane/water mixture always remaining at above 98%, indicating a good recyclability of the as-prepared meshes. Furthermore, multi-scale CuBTC-coated mesh was ultrasonicated with 200 W for 1 h. The UOCAs and separation efficiencies were measured at every 20 minutes. As shown in Figure 3c, the underwater superoleophobicity and separation efficiency of the mesh remained virtually unchanged after ultrasonication,

demonstrating the coating had a superior mechanical stability. The cooper mesh substrate offered additional metal source in the synthesis process, which enhanced the anchoring force between the coating and mesh. The chemical ability of multi-scale CuBTC-coated mesh was also tested by immersing the mesh into various organic solvents for 24 h and UOCAs were measured. As presented in Figure 3d, the mesh retained its underwater superoleophobicity and no obvious change of UOCA was observed after immersion, confirming the excellent chemical ability of the mesh. In a word, the obtained multi-scale CuBTC-coated meshes exhibited excellent stability and mechanical robustness, which would be beneficial for practical applications in separation of oil/water mixtures.

4.4. Comparison with literature reports

Furthermore, the performance of the oil/water separation mesh developed in this study was summarized in Figure 4, compared with the data reported in the literature. And the mesh substrate was used in all the compared study and this work. Obviously, multi-scale CuBTC-coated mesh prepared in this paper obtained the highest water flux with a satisfactory oil intrusion pressure simultaneously. The flux is positively correlated with water velocity (v) through the mesh, which can be determined by the following equation [29]:

$$v = \frac{\Delta P}{\mu R} \tag{4}$$

where ΔP is the pressure drop, μ the viscosity of the liquid, and R represents the resistance of mesh. Multi-scale CuBTC-coated mesh with a large pore size of about 65 μm generated relatively low resistance, thus relatively high flux (180.6 L $m^{-2} \cdot s^{-1}$) could be obtained. It was noteworthy that the calcined mesh exhibited a lower water flux (152 L $m^{-2} \cdot s^{-1}$) even though their pore sizes were similar (Figure 1g and S2a). The exceptional ultrahigh flux of the multi-scale CuBTC-coated mesh could be reasonably attributed to the substantial enhancement of the

hydrophilicity. In general, such a high water flux accompanied by a very low intrusion pressure as shown in Figure 4. However, our multi-scale CuBTC-coated mesh obtained a satisfactory intrusion pressure. The result benefited from a relatively thick water film formed on the prewetted multi-scale CuBTC-coated mesh and a relatively large UOCA. The reasons can be explained below.

According to Young-Laplace equation, due to the similar pore sizes of calcined mesh and multi-scale CuBTC-coated mesh, $\frac{P_2}{P_1} \approx \frac{\cos\theta_{ow2}}{\cos\theta_{ow1}}$ could be obtained, where θ_{ow1} is the UOAC of calcined mesh (Figure S4b) and θ_{ow2} represents the UOAC of multi-scale CuBTC mesh (Figure 2f). And the theoretical value of $\frac{P_2}{P_1}$ was about 1.3. Yet, the measured P_1 and P_2 were 0.77 and 2.2 kPa respectively, and the experimental $\frac{P_2}{P_1}$ value was 2.9. It could be assumed that an important factor besides UOCA led to a satisfactory intrusion pressure of multi-scale CuBTC-coated mesh in spite of a big mesh pore, and the relatively thick water film formed on the prewetted multi-scale CuBTC-coated mesh was speculated as the important factor. To verify this speculation, the water capture percentage (WCP), positively correlated with the thickness of water film, was measured based on eq 5.

$$C\,(\%) = \frac{W_{\mathrm{b}} - W_a}{W_{\mathrm{a}}} \times 100 \tag{5}$$

where C represents the WCP, W_{a} is the original mass of the mesh, W_{b} stands for the mass of the mesh after immersed in water and then quickly taken out from water. In this case, the WCP value of the prewetted multi-scale CuBTC-coated mesh was 54%, while the WCP value of the prewetted calcined mesh was 29%. Such a difference perhaps resulted in the difference between the two intrusion pressures to a great extent. To confirm this, the intrusion pressure was

measured with respect to the decreasing of the WCP. As shown in Figure S7, the intrusion pressure decreased with the decrease of WCP, namely, the intrusion pressure declined with the decrease of water film thickness. Here, CuBTC as a porous and hydrophilic material could capture more water molecules than other hydrophilic materials, which was beneficial to a higher intrusion pressure. Besides, a large UOCA of multi-scale CuBTC-coated meshes also contributed to the intrusion pressure. Based on the above conditions, it is not surprising that the prepared multi-scale CuBTC-coated mesh obtained such an unprecedentedly water flux with a satisfactory oil intrusion pressure simultaneously. Thanks to this, the as-prepared mesh could achieve ultrafast water transportation without worrying about oil breaking through.

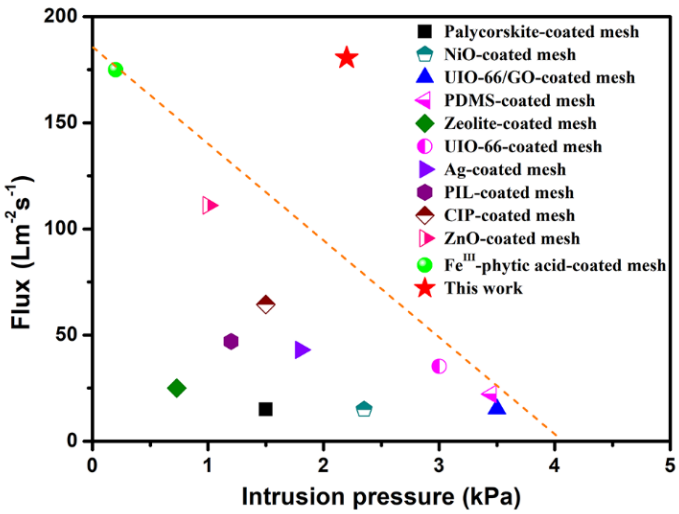

Figure 4. Comparison of previously literature oil/water separation performance with the results of this study (Palycorskite-coated mesh [9], NiO-coated mesh [10], zeolite-coated mesh [11], Ag-coated mesh [12], PIL-coated mesh [13], CIP-coated mesh [14], Fe^{III}-phytic acid-coated mesh [16], UIO-66/GO-coated mesh [17], UIO-66-coated mesh [18], PDMS-coated mesh [19], ZnO-coated mesh [20]).

4.5. Anti-fouling performances

As the prepared multi-scale CuBTC-coated mesh was aimed at collecting spilled oil, one concern maybe that the porous mesh might be blocked by the crude oil and then lose its separate ability. Therefore, an anti-fouling test was performed to verify the self-cleaning ability against crude oil of the multi-scale CuBTC-coated mesh, as shown in Figure 5. After the mesh was smudged and fouled by crude oil, water flow rinsed away the crude oil immediately, and the surface became thoroughly clean again. The magnified image of a multi-scale CuBTC-coated mesh after rinsing the adhered crude oil was shown in Figure S8, exhibiting there was no residual oil on the mesh. As mentioned above, when the CuBTC coating came in contact with the oil droplets, water pockets in the rough multi-scale micro-/nano-structures resulted in a large UOCA, providing a strong repulsive force. Therefore, such underwater superoleophobic properties could effectively prevent multi-scale CuBTC-coated meshes to be polluted or blocked up by oils during the oil/water separation process.

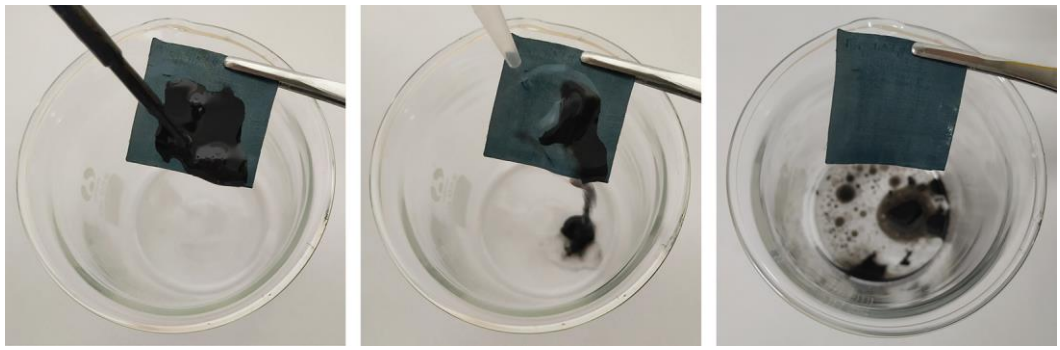

Figure 5. Anti-fouling performance of prepared multi-scale CuBTC-coated mesh against crude oil.

5. Conclusions

We successfully fabricated a multi-scale CuBTC-coated mesh by LPE procedure with secondary growth. The as-prepared CuBTC-coated mesh possessed superhydrophilicity and underwater superoleophobicity with the WCA of ca. 0° and the UOCA of ca. 162° attributed to

the inherent hydrophilicity of CuBTC coating with the multi-scale micro-/nano-structure. It exhibited a high separation efficiency of over 99% with respect to selective water separation from oil/water mixtures, which could maintain over 98% after 100 separation cycles. It was demonstrated that the as-prepared multi-scale CuBTC coating had a good mechanical stability with the excellent self-cleaning ability against crude oil under water. The unprecedentedly high permeation flux (180.6 $L \cdot m^{-2} \cdot s^{-1}$) was achieved with a satisfactory oil intrusion pressure (2.2 kPa), indicating the as-prepared multi-scale CuBTC-coated mesh could be applied for rapid separation of oil/water mixtures in large quantity.

6. Notes

The authors declare that they have no known competing financial interests or personal relationships that could have appeared to influence the work reported in this paper.

Acknowledgements

This work was financially supported by National Natural Science Foundation of China (U20A20152, 21136008).

Appendix A. Supplementary material

Supplementary data to this article can be found online at https://doi.org/

References

[1] M.A. Shannon, P.W. Bohn, M. Elimelech, J.G. Georgiadis, B.J. Mariñas, A.M. Mayes, Science and technology for water purification in the coming decades, Nature 452 (2008) 301–310. https://doi.org/10.1038/nature06599

[2] M. Schrope, Oil Spill: Deep wounds, Nature 472 (2011) 152–154. https://doi.org/10.1038/472152a

[3] B. Wang, W.X. Liang, Z.G. Guo, W.M. Liu, Biomimetic super-lyophobic and super-lyophilic materials applied for oil/water separation: a new strategy beyond nature, Chem. Soc. Rev. 44 (2015) 336–361. https://doi.org/10.1039/c4cs00220b

[4] Q.L. Ma, H.F. Cheng, A.G. Fane, R. Wang, H. Zhang, Recent development of advanced materials with special wettability for selective oil/water separation, Small 12 (2016) 2186–2202. https://doi.org/10.1002/smll.201503685

[5] Z.L. Chu, Y.J. Feng, S. Seeger, Oil/water separation with selective superantiwetting/superwetting surface materials, Angew. Chem. Int. Ed. 54 (2015) 2328–2338. https://doi.org/10.1002/anie.201405785

[6] Y. Li, X.Z. Shang, B.Q. Zhang, One-step fabrication of the pure-silica zeolite beta coating on stainless steel mesh for efficient oil/water separation, Ind. Eng. Chem. Res. 57 (2018) 17409–17416. https://doi.org/10.1021/acs.iecr.8b04172

[7] C.L. Chen, D. Weng, A. Mahmood, S. Chen, J.D. Wang, Separation mechanism and construction of surfaces with special wettability for oil/water separation, ACS Appl. Mater. Interfaces 11 (2019) 11006−11027. https://doi.org/10.1021/acsami.9b01293

[8] S.J. Gao, J.C. Sun, P.P. Liu, F. Zhang, W.B. Zhang, S.L. Yuan, J.Y. Li, J. Jin, A robust polyionized hydrogel with an unprecedented underwater anti-crude-oil-adhesion property, Adv. Mater. 28 (2016) 5307−5314. https://doi.org/10.1002/adma.201600417

[9] J. Li, L. Yan, H.Y. Li, W.J. Li, F. Zha, Z.Q. Lei, Underwater superoleophobic palygorskite coated meshes for efficient oil/water separation, J. Mater. Chem. A 3 (2015) 14696−14702. https://doi.org/10.1039/c5ta02870a

[10] Z.W. Yu, F.F. Yun, Z.Y. Gong, Q. Yao, S.X. Dou, K.S. Liu, L. Jiang, X.L. Wang, A novel reusable superhydrophilic NiO/Ni mesh produced by a facile fabrication method for superior oil/water separation, J. Mater. Chem. A 5 (2017) 10821−10826. https://doi.org/10.1039/c7ta01987d

[11] Q. Wen, J.C. Di, L. Jiang, J.H. Yu, R.R. Xu, Zeolite-coated mesh film for efficient oil–water separation, Chem. Sci. 4 (2013) 591−595. https://doi.org/10.1039/c2sc21772d

[12] L.Y. Liu, C. Chen, S.Y. Yang, H. Xie, M.G. Gong, X.L. Xu, Fabrication of superhydrophilic-underwater superoleophobic inorganic anti-corrosive membranes for high-efficiency oil/water separation, Phys. Chem. Chem. Phys. 18 (2016) 1317−1325. https://doi.org/10.1039/c5cp06305a

[13] Y.Y. Zhang, X. Deng, L.R. Zhang, B.H. Chen, T. Ding, B. Ni, G.H. Gao, Swelling poly(Ionic liquid) supported by three-dimensional wire mesh for oil/water separation. ACS Appl Mater. Interfaces 11 (2019) 14347−14353. https://doi.org/10.1021/acsami.9b02085

[14] M. Joo, J. Shin, J. Kim, J.B. You, Y. Yoo, M.J. Kwak, M.S. Oh, S.G. Im, One-step synthesis of cross-linked ionic polymer thin films in vapor phase and its application to an oil/water separation membrane, J. Am. Chem. Soc. 139 (2017) 2329−2337. https://doi.org/10.1021/jacs.6b11349

[15] Y. Dong, J. Li, L. Shi, X.B. Wang, Z.G. Guo, W.M. Liu, Underwater superoleophobic graphene oxide coated meshes for the separation of oil and water, Chem. Commun. 50 (2014) 5586−5589. https://doi.org/10.1039/c4cc01408a

[16] L.B. Li, G.Y. Zhang, Z.H. Su, One-step assembly of phytic acid metal complexes for superhydrophilic coatings, Angew. Chem. Int. Ed. 55 (2016) 9093−9096. https://doi.org/10.1002/anie.201604671

[17] H. Li, Y.Y. Yin, L. Zhu, Y. Xiong, X. Li, T.C. Guo, W. Xing, Q.Z. Xue, A hierarchical structured steel mesh decorated with metal organic framework/graphene oxide for high-efficient oil/water separation, J. Hazard. Mater. 373 (2019) 725−732. https://doi.org/10.1016/j.jhazmat.2019.04.009

[18] X.J. Zhang, Y.X. Zhao, S.J. Mu, C.M. Jiang, M.Q. Song, Q.R. Fang, M. Xue, S.L. Qiu, B.L. Chen, UiO-66-coated mesh membrane with underwater superoleophobicity for high-efficiency oil–water separation, ACS Appl. Mater. Interfaces 10 (2018) 17301−17308. https://doi.org/10.1021/acsami.8b05137

[19] N. Wen, X.R. Miao, X.J. Yang, M.Y. Long, W.S. Deng, Q.N. Zhou, W.L. Deng, An alternative fabrication of underoil superhydrophobic or underwater superoleophobic stainless steel meshes for oil-water separation: originating from one-step vapor deposition of polydimethylsiloxane, Sep. Purif. Technol. 204 (2018) 116−126. https://doi.org/10.1016/j.seppur.2018.04.059

[20] A. Huang, C.-C. Kan, S.-C. Lo, L.-H. Chen, D.-Y. Su, J.F. Soesanto, C.-C. Hsu, F.-Y. Tsai, K.-L. Tung, Nanoarchitectured design of porous ZnO@copper membranes enabled by atomic-layer-deposition for oil/water separation, J. Member. Sci. 582 (2019) 120−131. https://doi.org/10.1016/j.memsci.2019.03.093

[21] J. Liu, L. Wang, N. Wang, F.Y. Guo, L. Hou, Y.E. Chen, J.C. Liu, Y. Zhao, L. Jiang, A robust $Cu(OH)_2$ nanoneedles mesh with tunable wettability for nonaqueous multiphase liquid separation, Small 13 (2017) 1600499. https://doi.org/10.1002/smll.201600499

[22] S.S. Yuan, J.Y. Zhu, Y. Li, Y. Zhao, J. Li, P.V. Puyvelde, B.V. Bruggen, Structure architecture of micro/nanoscale ZIF-L on a 3D printed membrane for a superhydrophobic and underwater superoleophobic surface, J Mater. Chem. A 7 (2019) 2723–2729. https://doi.org/10.1039/c8ta10249j

[23] S.S.-Y. Chui, S.M.-F. Lo, J.P.H. Charmant, A.G. Orpen, I.D. Williams, A chemically functionalizable nanoporous material $[Cu_3(TMA)_2(H_2O)_3]_n$, Science 283 (1999) 1148–1150. https://doi.org/10.1126/science.283.5405.1148

[24] K. Schlichte, T. Kratzke, S. Kaskel, Improved synthesis, thermal stability and catalytic properties of the metal-organic framework compound $Cu_3(BTC)_2$, Micropor. Mesopor. Mater. 73 (2004) 81–88. https://doi.org/10.1016/j.micromeso.2003.12.027

[25] M.M. Liu, L. Tie, J. Li, Y.Y. Hou, Z.G. Guo, Underoil superhydrophilic surfaces: water adsorption in metal–organic frameworks, J. Mater. Chem. A 6 (2018) 1692–1699. https://doi.org/10.1039/c7ta09711e

[26] H.L. Guo, G.S. Zhu, I.J. Hewitt, S.L. Qiu, "Twin copper source" growth of metal-organic framework membrane: $Cu_3(BTC)_2$ with high permeability and selectivity for recycling H_2, J. Am. Chem. Soc. 131 (2009) 1646–1647. https://doi.org/10.1021/ja8074874

[27] Q. Ma, G.D. Li, X.Y. Liu, Z. Wang, Z. Song, H.T. Wang, Zeolitic imidazolate framework-8 film coated stainless steel meshes for highly efficient oil/water separation, Chem. Commun. 54 (2018) 5530−5533. https://doi.org/10.1039/c8cc01515e

[28] W.S. Chi, B.J. Sundell, K. Zhang, D.J. Harrigan, S.C. Hayden, Z.P. Smith, Mixed-matrix membranes formed from multi-dimensional metal organic frameworks for enhanced gas transport and plasticization resistance, ChemSusChem 12 (2019) 2355−2360. https://doi.org/10.1002/cssc.201900623

[29] A. Rushton, A.A. Ward, R.G. Holdich, Filtration fundamentals. Solid-Liquid Filtration and Separation Technology, 1rd ed., Wiley, Weinheim, 1996, pp. 6–7. https://doi.org/10.1002/9783527614974.ch01